Inorganic Chemistry

Article

pubs.acs.org/IC

Preparation and Instability of Nanocrystalline Cuprous Nitride

Malinda D. Reichert, Miles A. White, Michelle J. Thompson, Gordon J. Miller, and Javier Vela*

Department of Chemistry, Iowa State University and Ames Laboratory, Ames, Iowa 50011, United States

Supporting Information

ABSTRACT: Low-dimensional cuprous nitride (Cu_3N) was synthesized by nitridation (ammonolysis) of cuprous oxide (Cu_2O) nanocrystals using either ammonia (NH_3) or urea (H_2NCONH_2) as the nitrogen source. The resulting nanocrystalline Cu_3N spontaneously decomposes to nanocrystalline CuO in the presence of both water and oxygen from air at room temperature. Ammonia was produced in 60% chemical yield during Cu_3N decomposition, as measured using the colorimetric indophenol method. Because Cu_3N decomposition requires H_2O and produces substoichiometric amounts of NH_3, we conclude that this reaction proceeds through a complex stoichiometry that involves the concomitant release of both N_2 and NH_3. This is a thermodynamically unfavorable outcome, strongly indicating that H_2O (and thus NH_3 production) facilitate the kinetics of the reaction by lowering the energy barrier for Cu_3N decomposition. The three different Cu_2O, Cu_3N, and CuO nanocrystalline phases were characterized by a combination of optical absorption, powder X-ray diffraction, transmission electron microscopy, and electronic density of states obtained from electronic structure calculations on the bulk solids. The relative ease of interconversion between these interesting and inexpensive materials bears possible implications for catalytic and optoelectronic applications.

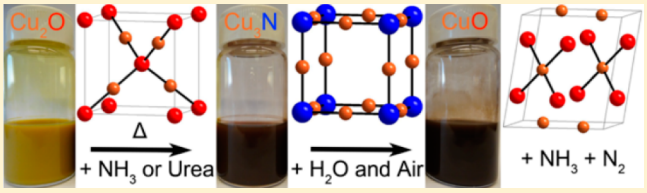

INTRODUCTION

Copper(I) nitride (Cu_3N) is a metastable semiconductor that has a low reflectivity and high electrical resistivity.[1] It has been reported to have a narrow experimental band gap of 1.2−1.9 eV[2] and features a cubic anti-ReO_3 structure.[3] Because of these properties, Cu_3N nanocrystals (NCs) are promising materials for optical storage devices, random access memory chips, conductive inks, high-speed integrated circuits, microscopic metal links, photocatalysts, and electrocatalytic hydrogen reduction devices.[1−3]

Cu_3N NCs can be synthesized by several methods. Cu_3N nanocubes were synthesized by the one-pot decomposition of copper(II) nitrate in octadecene, octadecylamine, and oleylamine.[1,2,4,5] Copper nitride nanocrystals were also produced by decomposing $Cu(OAc)_2$ with ammonia,[3,6−9] a metastable $CuCl_2$-sodium azide precursor,[10] or $\{[Cu_5(CN)_6(NH_3)_6(N_3)_2]\}_n$.[11] Cu_3N nanopowders were produced by ammonolysis of CuF_2.[12] Cu_4N and Cu_3N_2 nanostructures have been prepared as thin films.[13−16]

A versatile route for making nitrides and oxynitrides is the nitridation (ammonolysis) of metal oxides. CuO has been used as a precursor to Cu_3N. Silica-supported CuO nanoparticles were converted to Cu_3N by nitridation with ammonia.[17] Nitridation of sol−gel CuO with ammonia produced silica-supported Cu_3N nanocrystals.[18] Ammonia is believed to reduce CuO to a zerovalent (metallic) copper intermediate during nitride formation.[19]

Cupric (Cu^{2+}) and cuprous (Cu^{+}) oxide nanocrystals are well described in the literature. The synthesis, characterization, and optoelectronic properties of CuO nanostructures have been reviewed.[20,21] Like CuO nanocrystals, nitridation of Cu_2O nanocrystals could also lead to Cu_3N. Controlled syntheses (monodispersity, size, morphology) of Cu_2O nanocrystals by electrodeposition, wet chemical, and solvothermal methods exist, along with reports on their surface, catalytic, and electrical properties.[20,22,23]

An interesting feature of Cu_3N is its documented decomposition upon heating or electron bombardment. For example, Cu_3N thin films convert to CuO nanowire arrays by annealing in air.[24] Cu_3N deposited by magnetic sputtering converts to Cu and N_2 under electron bombardment or by annealing in a vacuum.[25,26] The optical properties of Cu_3N thin films made by ion-assisted deposition remained unchanged upon conducting an aging test at 60 °C and 95% humidity for 15 months, but degraded to copper metal when heated to 300 °C.[27] Cu_3N nanoparticles were reported to degrade thermally, forming CuO at temperatures ranging between 200 and 330 °C under an argon atmosphere.[3]

In this work, we synthesize Cu_3N nanocrystals by nitridation of Cu_2O nanocrystals with either ammonia or urea. We characterize the structure, optical properties, and morphology of both oxide and nitride phases using structural, optical, and computational methods. We also describe the spontaneous room-temperature decomposition of Cu_3N nanocrystals upon exposure to moisture and air, and used simple thermodynamics calculations to explain that the observed concomitant release of NH_3 and N_2 is due to kinetic factors.

Received: March 26, 2015
Published: June 19, 2015

DOI: 10.1021/acs.inorgchem.5b00679
Inorg. Chem. 2015, 54, 6356−6362

EXPERIMENTAL SECTION

Materials. Copper(II) chloride dihydrate ($CuCl_2·2H_2O$, 99.0%) and sodium nitroprusside dihydrate ($Na_2[Fe(CN)_5NO]·2H_2O$, 99.0%) were purchased from Sigma-Aldrich; ammonium carbonate ($(NH_4)_2CO_3$, tech.), ascorbic acid ($C_6H_8O_6$, tech.), and sodium hydroxide (NaOH, tech.) from Fisher; urea (H_2NCONH_2, tech.) and phenol (C_6H_5OH, tech.) from Alfa Aesar; ammonia gas (NH_3, 99.99%) from Airgas; and sodium hypochlorite (NaOCl, 8.25%) from Clorox. All chemicals were used as received.

Synthesis. *Cu_2O Nanocrystals.* Cu_2O nanocrystals were made by a modified literature procedure:[28] Briefly, 100 mL of a 0.4 M NaOH solution was added to 100 mL of a 0.2 M $CuCl_2$ solution. After the solution was stirred for 5 min, 100 mL of a 0.2 M $C_6H_8O_6$ was added. The mixture was stirred for 25 min and centrifuged. The precipitate was collected, washed three times with distilled water and once with ethanol, and dried at room temperature (R.T., ca. 21−24 °C) for 12 h. *Cu_3N nanocrystals from ammonia.* Cu_2O nanocrystals (0.15 g) were placed in an alumina combustion boat and put in a fused silica tube inside of a tube furnace (Lindberg 55035). The tube was purged with NH_3 (60 mL/min) for 30 min and then heated to 250 °C for 21 h. *Cu_3N nanocrystals from urea.* Cu_2O nanocrystals (0.15 g) were weighed along with H_2NCONH_2 (0.126 g) into a Teflon liner inside a 23 mL steel autoclave. The autoclave was placed in a Thomas Scientific (5300A25) muffle furnace and heated to 190 °C (10 °C/min ramp rate, 6 h dwell time). *CuO from Cu_3N decomposition.* Cu_3N (∼100 mg, synthesized using either NH_3 or H_2NCONH_2) was exposed to deionized water (10 mL) for 15 days. The product was isolated by centrifugation (4500 rpm, 10 min). To determine the amount of ammonia released during the Cu_3N decomposition reaction, we used the *indophenol method.*[29,30] *Solution A:* C_6H_5OH (5 g, 53 mmol) and $Na_2[Fe(CN)_5NO]·2H_2O$ (0.025 g, 0.084 mmol) were dissolved in deionized water (500 mL) using a volumetric flask. *Solution B:* NaOH (2.5 g, 62.5 mmol) was dissolved in deionized water, NaOCl (8.25%, 4.2 mL) added, and solution diluted with deionized water to 500 mL in a volumetric flask. The two solutions were stored in amber bottles at ca. 8−10 °C using a refrigerator and used within 2 weeks. Seven different calibration solutions were made using solution A (5 mL) and a 0.5 mM solution of $(NH_4)_2CO_3$ in deionized water (0 to 350 μL in 50 μL increments). Solution B (5 mL) was added and the mixture was stirred at 37 °C for 20 min. Absorbance values at λ = 623 nm were used to construct the calibration curve. After centrifugation to isolate the CuO during Cu_3N decomposition, the same indophenol method was used to analyze the supernatant solutions (100 μL) for NH_3 content. Values reported are three-run averages.

Structural Characterization. *X-ray Diffraction.* Powder X-ray diffraction (XRD) data were measured using Cu Kα radiation on a Rigaku Ultima U4 difractometer. Sample percent composition was determined using PowderCell 2.4 (PCW) refined against standard XRD patterns for Cu_2O, Cu_3N, and CuO. Single-crystalline domain sizes were calculated using the Scherrer equation and the typical uncertainty estimated to be ±0.2 nm. *Transmission Electron Microscopy.* Transmission electron microscopy (TEM) was conducted on carbon-coated copper grids using a FEI Tecnai G2 F20 field emission scanning transmission electron microscope (STEM) at 200 kV (point-to-point resolution <0.25 nm, line-to-line resolution <0.10 nm). Particle dimensions were measured manually and/or by using ImageJ. Size measurements and particle statistics were obtained for at least >100 particles. Average sizes ± standard deviations are reported.

Optical Characterization. Absorption spectra were measured using a photodiode array Agilent 8453 UV−vis spectrophotometer. Solvent absorption was subtracted from all spectra. Diffuse reflectance measurements were made using a StellarNet Inc. Black-Comet-SR spectrometer (200−1080 nm).

Density of States (DOS) Calculations. Electronic structure calculations of CuO, Cu_2O, and Cu_3N were performed using the Vienna *Ab initio* Simulation Package (VASP).[31,32] All VASP calculations were performed using projected augmented-wave (PAW) pseudopotentials with a cutoff energy of 500 eV and a convergence energy of 1×10^{-6} eV.[33] A conjugated algorithm was applied for the structural optimization with a 15 × 15 × 15 Monkhorst-pack k-points grid.[34] During structure optimization, atomic coordinates and cell volumes were allowed to optimize. Total energies were calculated using the tetrahedron method with Blöchl[35] corrections applied. All VASP calculations treated exchange and correlation by the Perdew-Burke-Enzerhoff (PBE) method.[36] Because of the highly correlated nature of these compounds, on-site Coulomb interactions were used (LDA + U). The *U* value applied was 5.0 eV for the Cu d states due to this value being successful for previous studies on strongly correlated Cu compounds.[37,38]

RESULTS AND DISCUSSION

Synthesis of Cu_2O Nanocrystals. On the basis of previous reports of successful nitridation of CuO, we attempted to perform a similar reaction using nanocrystalline Cu_2O as the starting material. We first synthesized Cu_2O nanocrystals by reacting copper(II) chloride and sodium hydroxide using a modified literature procedure.[28] This reaction proceeds through a blue copper-hydroxide intermediate, which upon treatment with ascorbic acid produces an orange solution of Cu_2O. X-ray diffraction confirmed the formation of cubic copper(I) oxide (Cu_2O) nanocrystals (Figures 1 and 2a). The unit cell of Cu_2O

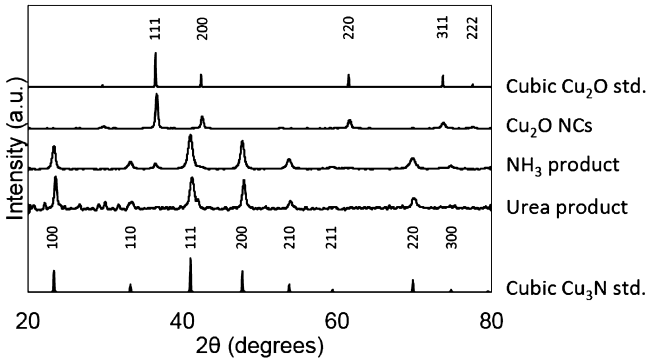

Figure 1. Experimental powder XRD patterns before and after treating Cu_2O nanocrystals with ammonia (NH_3) or urea (H_2NCONH_2). Reported powder XRD patterns for bulk cubic Cu_2O and cubic (anti-ReO_3) Cu_3N are shown for comparison.

consists of a body-centered cubic (bcc) arrangement of oxide ions (O^{2-}) with two-coordinate cuprous ions (Cu^+) linking every second corner with the central oxide (Figure 2a). The size of the Cu_2O nanocrystals, as estimated from XRD peak widths using the Scherrer equation, is approximately 25 nm. Figure 3 shows the general appearance and optical absorption of the Cu_2O nanocrystals. Absorption starts at 600 nm for both the diffuse reflectance of a solid film and the solution phase absorption spectrum of the Cu_2O nanocrystals, which roughly agree with a reported experimental Cu_2O band gap of 2.2 eV (see calculated vs experimental band gap discussion below).[28] TEM shows that the Cu_2O nanocrystals have a cubic morphology, with an average size of 43 ± 10 nm (Figure 4). Table 1 summarizes these observations.

Nitridation of Cu_2O Nanocrystals. We used two different reagents to nitride nanocrystals of Cu_2O to produce Cu_3N, namely, ammonia (NH_3) and urea (H_2NCONH_2) (eqs 1 and 2, respectively, in Scheme 1). XRD shows that, in both cases, the main product is made of anti-ReO_3 Cu_3N nanocrystals with Scherrer sizes of 15 nm (NH_3) and 22 nm (urea) (Figure 1 and Table 1). The cubic, anti-ReO_3-type unit cell of Cu_3N consists of a primitive cubic arrangement of nitride ions with two-coordinate cuprous ions linking every two neighboring nitrides

DOI: 10.1021/acs.inorgchem.5b00679
Inorg. Chem. 2015, 54, 6356−6362

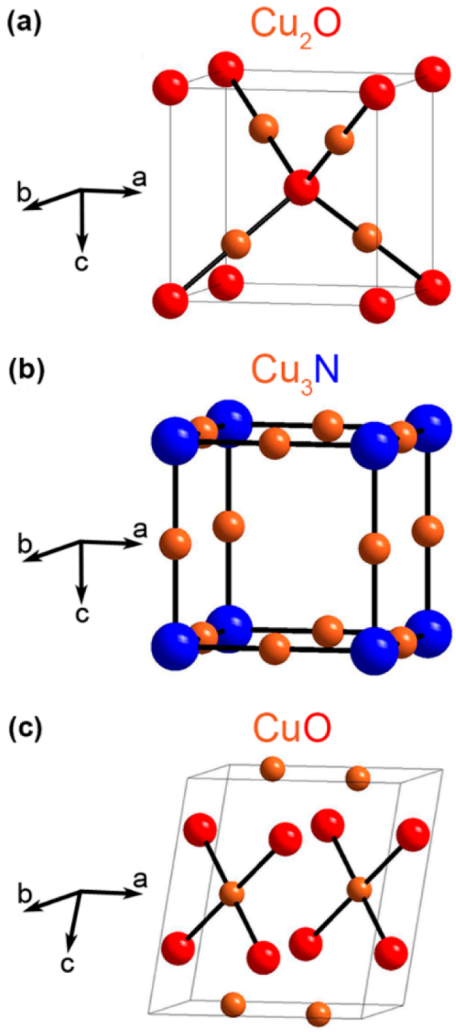

Figure 2. Crystalline unit cells for cubic (a = 4.27 Å) (cuprite) Cu_2O (a), cubic (a = 3.81 Å) (anti-ReO_3) Cu_3N (b), and monoclinic (a = 4.68 Å, b = 3.47 Å, c = 5.12 Å, and β = 99.7°) (tenorite) CuO (c).

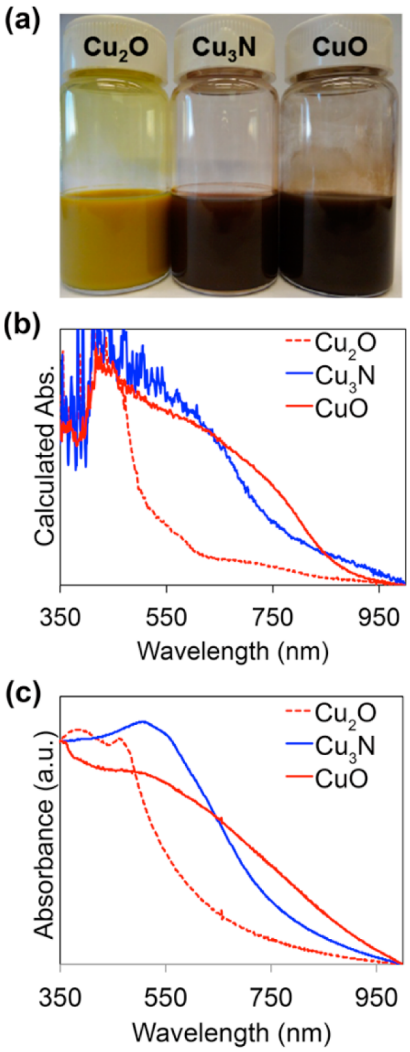

Figure 3. General appearance (suspended in methanol) (a), solid phase diffuse reflectance (b), and solution phase electronic absorption spectra (in methanol) (c) of nanocrystalline Cu_2O, Cu_3N, and CuO.

(Figure 2b). The product of nitridation with ammonia contains some unreacted Cu_2O (6%), while the product of nitridation with urea contains smaller amounts of Cu_2O (1.6%) and CuO (0.4%) (Table 1). Figure 3 shows diffuse reflectance (solid) and optical absorption (solution) spectra of the Cu_3N nanocrystals made using ammonia as the nitridation agent as a representative example. These nanocrystals show an absorption band edge of around 700 nm, which very roughly matches different reports of experimental Cu_3N band gaps between 1.1 eV and 1.9 eV.[39] The absorption spectra of the reddish-brown Cu_3N nanocrystals in both solid form and in solution demonstrate this red shifting (Figure 3b,c). TEM measurements indicate a reagent-dependent change in nanocrystal morphology upon nitridation. Nitridation with ammonia leads to aggregated, spheroidal Cu_3N nanocrystals with a size of 22 ± 7 nm (Figure 4b and Table 1). Nitridation with urea leads to aggregated Cu_3N nanocrystals with a wider range of morphologies, including rods, sheets, and clusters with sizes of 370 ± 160 nm, 310 ± 160 nm, and 220 ± 140 nm, respectively (Figure 4d and Table 1).

Electronic Structure Calculations. To gain more insight into the optical properties of the different nanocrystalline copper phases presented here, we performed first-principles

Scheme 1

$$Cu_2O_{(s)} + NH_{3(g)} \xrightarrow[21\ h]{250\ ^\circ C} Cu_3N_{(s)} \quad \text{(unbalanced)} \quad (1)$$

$$Cu_2O_{(s)} + (NH_2)_2CO_{(g)} \xrightarrow[6\ h]{190\ ^\circ C} Cu_3N_{(s)} \quad \text{(unbalanced)} \quad (2)$$

electronic structure calculations on bulk solids to obtain electronic DOS curves (Figure 5). Cu_2O and Cu_3N both display similar electronic structures. In both species, a band gap is present at the Fermi level with a magnitude of 0.95 and 0.73 eV for Cu_3N and Cu_2O, respectively. This value agrees well with previously reported calculations: Cu_2O is similar to prior calculations that reported a theoretical value of 0.78;[40] Cu_3N calculations claimed band gaps that were generally smaller but ranged in theoretical value from 0.23 to 0.9 eV.[41] Our calculated band gap for Cu_3N agrees well with experimental values, while the Cu_2O band gap is much smaller than those obtained experimentally. An explanation for this discrepancy is the difference between electronic and optical band gaps in Cu_2O. Previous work has found that the direct transition at Γ is forbidden, which leads to no appreciable optical absorption until above 2 eV.[42]

DOI: 10.1021/acs.inorgchem.5b00679
Inorg. Chem. 2015, 54, 6356−6362

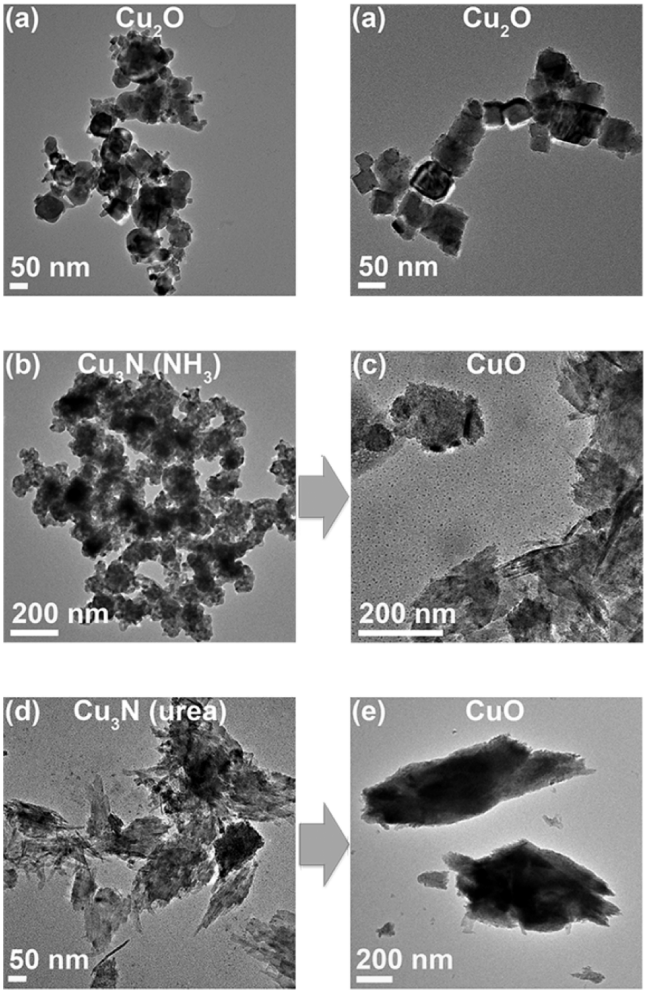

Figure 4. Representative TEM micrographs of nanocrystalline Cu_2O (a), Cu_3N made from NH_3 (b) and its decomposition product (c), and Cu_3N made from urea (d) and its decomposition product (e).

Spontaneous Decomposition of Cu_3N to CuO. During the humid summer time, we observed spontaneous decomposition of the Cu_3N nanocrystals over a period of several days. To track their fate, we characterized the product using powder XRD, and determined that it was made of nanocrystalline monoclinic (tenorite) CuO (Figure S1, Scheme 2). The tenorite CuO unit cell contains tetracoordinate cupric (Cu^{2+}) ions in an approximately square planar configuration (Figure 2c). Scherrer particle sizes obtained from XRD are 16 and 12 nm for CuO nanocrystals derived from NH_3- and urea-made Cu_3N, respectively. TEM shows that the CuO produced is made of highly aggregated clusters (100−140 nm) of small nanocrystals (13 ± 3 nm) (Figure 4c,e and Table 1).

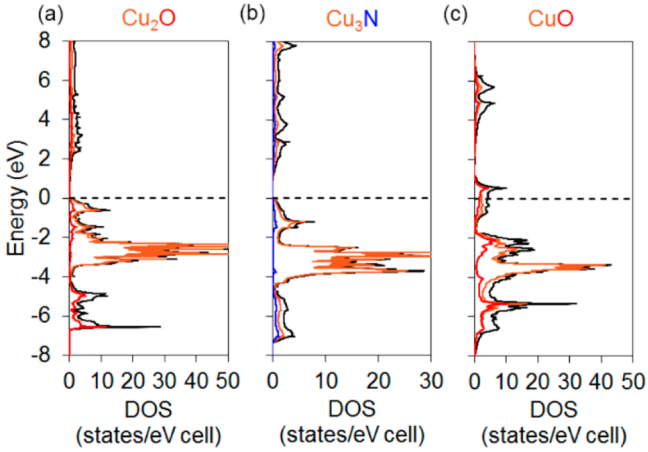

Figure 5. Density of state (DOS) curves for Cu_2O (a), Cu_3N (b), and CuO (c). Total DOS is depicted in black. Partial DOS (pDOS) are given in copper (Cu), red (O), and blue (N).

Reported experimental band gap values for CuO lie in the 1.2−1.5 eV range (see below).[43,44] The black-colored CuO produced here has a slightly redder absorption edge (ca. 850 nm) than Cu_3N (Figure 5). DOS calculations show that the electronic structure of CuO is much more complicated than Cu_2O or Cu_3N (Figure 5). The most notable feature of the DOS curve for CuO is the peak located at the Fermi level. In traditional band theory, this would indicate CuO is metallic. Along with CoO and NiO, CuO belongs to a class of late metal oxides known as Mott insulators. In addition to the strong Coulombic interactions mentioned above, a recent investigation, focused on elucidating the electronic structure of CuO, found that spin−orbit coupling (SOC) also plays an important role.[45] Without SOC, the valence band ends 1.17 eV above the Fermi level, after which there is a small gap of 0.49 eV, consistent with prior theoretical estimates.[41] However, calculations accounting for SOC found the band gap to start at the Fermi level and be 1.2 eV in magnitude.[45] This value agrees better with experimental values and supports the claim that SOC is an important factor for this class of compounds.

To elucidate what caused the decomposition of Cu_3N nanocrystals, we attempted to react them with water under

Table 1. Synthesis and Instability Studies of Cuprous Nitride Nanocrystals

			dimensions (nm)		
no.	precursors	conditions	XRD	TEM	XRD phase(s) (% composition)[c]
1	$CuCl_{2(aq)}$ + NaOH + $C_6H_8O_6$[a]	R.T.,[b] 20 min	25	43 ± 10	cubic Cu_2O (100)
2	Cu_2O + $NH_{3(g)}$	250 °C, 21 h	15	22 ± 7	cubic (anti-ReO_3) Cu_3N (94) + cubic Cu_2O (6)
3	Cu_2O + H_2NCONH_2 (urea)	190 °C, 6 h	22	370 ± 160 (rods) 310 ± 160 (sheets) 220 ± 140 (aggregates)	cubic (anti-ReO_3) Cu_3N (98) + cubic Cu_2O (1.6) + monoclinic (tenorite) CuO (0.4)
4	Cu_3N (from NH_3) + H_2O + O_2 (air)	R.T.,[b] 15 days	16	13 ± 3 (dots) 140 ± 60 (aggregates)	monoclinic (tenorite) CuO (99.1) + cubic Cu_2O (0.7) + cubic (anti-ReO_3) Cu_3N (0.2)
5	Cu_3N (from urea) + H_2O + O_2 (air)	R.T.,[b] 15 days	12	100 ± 70 (aggregates)	CuO monoclinic (100)

[a]Ascorbic acid. [b]21−24 °C. [c]Sample percent composition was determined using PowderCell 2.4 (PCW) refined against standard XRD patterns for Cu_2O, Cu_3N, and CuO.

DOI: 10.1021/acs.inorgchem.5b00679
Inorg. Chem. 2015, 54, 6356−6362

argon (oxygen-free), with dry oxygen (water-free), or with water and oxygen together as control experiments (eqs 3, 4, and 5, respectively, in Scheme 2). As shown in Figure 6,

Scheme 2

$$Cu_3N_{(s)} + H_2O_{(l)} \xrightarrow[15\ days]{RT\ /\ Ar} \text{Slow or no reaction} \quad (3)$$

$$Cu_3N_{(s)} + O_{2(g)} \xrightarrow[15\ days]{RT} \text{Slow or no reaction} \quad (4)$$

$$Cu_3N_{(s)} + H_2O_{(l)} + O_{2(g)} \xrightarrow[15\ days]{RT} CuO_{(s)} \quad \text{(unbalanced)} \quad (5)$$

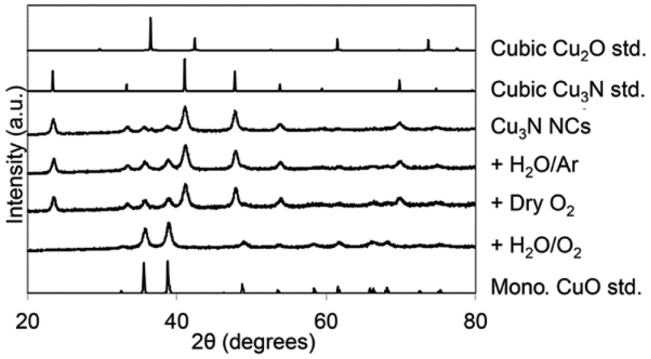

Figure 6. Experimental powder XRD patterns obtained before and after treating Cu_3N nanocrystals (NCs) with H_2O under Ar (O_2-free), dry O_2 (H_2O-free), and H_2O plus O_2. Reported powder XRD patterns for bulk cubic Cu_2O, cubic (anti-ReO_3) Cu_3N, and monoclinic (tenorite) CuO are shown for comparison (all reactions were performed at R.T. for 15 days).

treating Cu_3N nanocrystals with water under an oxygen-free Ar atmosphere at room temperature (R.T.) for 15 days did not result in any observable change. The same was true when dry (moisture-free) O_2 was used. In contrast, Cu_3N completely transformed to nanocrystalline CuO in the presence of both water and O_2 (Figure 6). This reproducible result is independent of the original nitridation source (NH_3 or urea) that was employed in making Cu_3N with very different sizes and morphologies. This result is also consistent with our observation that Cu_3N decomposition occurred faster during the humid summer months than during the dry winter months.

Tracing the Fate of Nitrogen after Cu_3N Decomposition. Two nonmutually exclusive, possible nitrogen-containing products of Cu_3N decomposition are ammonia (NH_3) and molecular nitrogen (N_2). We first suspected that NH_3 was produced after observing an increase in the pH of the original solution exposed to the Cu_3N nanocrystals from slightly acidic or neutral before reaction, to basic after the decomposition of Cu_3N to CuO was complete. To further examine this issue, we sought to confirm whether NH_3 was produced and, if so, to measure exactly how much NH_3 was produced, using the colorimetric indophenol method (eq 6 in Scheme 3 and Figure S2).[46,47] As shown in Table 2, similar amounts of ammonia were released upon Cu_3N decomposition regardless of the source of nitrogen originally used for nitridation (NH_3 or urea). In all cases, the experimentally measured chemical yield of NH_3 remained constant and equal to 60% relative to the initial amount of Cu_3N.

Scheme 3. Colorimetric Indophenol Quantification of NH_3

$$NH_{3(aq)} \xrightarrow[(b)\ NaOPh,\ Na_2[Fe(CN)_5NO]]{(a)\ HOCl} \text{Indophenol blue} \quad (6)$$

Table 2. Colorimetric Determination of NH_3 Produced from Cu_3N Decomposition Using the Indophenol Method

	Cu_3N^a	NH_3	
	moles[a]	moles[b]	% yield[c]
Cu_3N (NH_3)	$5.13 \pm 0.07 \times 10^{-5}$	$3.27 \pm 0.04 \times 10^{-5}$	63.7 ± 0.9
Cu_3N (urea)	$5.33 \pm 0.05 \times 10^{-5}$	$2.98 \pm 0.04 \times 10^{-5}$	56 ± 1

[a]Decomposition reactions were carried out in 10 mL of deionized water. [b]Small, 100 μL aliquots were further diluted with 10 mL of deionized water to produce the solutions in Figure S2. [c]Based on the total amount of nitrogen (from Cu_3N).

Thermodynamic Rationale of CuO Formation. In principle, formation of N_2 or NH_3 from Cu_3N decomposition (oxidation to CuO) could be rationalized by either of the balanced eqs 7 or 8 (Scheme 4). The enthalpies of formation

Scheme 4

$$Cu_3N_{(s)} + {}^3/_2O_{2(g)} \xrightarrow{\Delta G_7} 3CuO_{(s)} + {}^1/_2N_{2(g)} \quad (7)$$

$$Cu_3N_{(s)} + {}^5/_2H_2O_{(l)} + {}^3/_4O_{2(g)} \xrightarrow{\Delta G_8} 3CuO_{(s)} + NH_4^+{}_{(aq)} + HO^-{}_{(aq)} \quad (8)$$

$$Cu_3N_{(s)} + {}^{5x}/_2H_2O_{(l)} + {}^{(6-3x)}/_4O_{2(g)} \xrightarrow{\Delta G_9} 3CuO_{(s)} + xNH_4^+{}_{(aq)} + xHO^-{}_{(aq)} + {}^{(1-x)}/_2N_{2(g)} \quad (9)$$

(ΔH_f) of all reactants and products in these equations are known, including those of Cu_3N (ΔH_f = 77 kJ/mol)[48,49] and CuO (ΔH_f = −157.3 kJ/mol)[50] (near standard conditions). Using these values, the enthalpies of reactions (ΔH_r) (7) and (8) are calculated to be −549 kJ/mol and −197 kJ/mol, respectively. Therefore, decomposition of Cu_3N exclusively to N_2 vs NH_3 (reaction 7 vs 8) is favored enthalpically by ca. 350 kJ/mol (Figure 7). In other words, there is an inverse relationship between the enthalpy of the Cu_3N decomposition

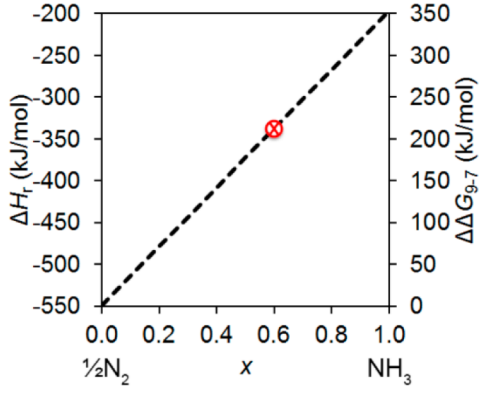

Figure 7. Change in enthalpy (ΔH_r) and free energy (ΔG_r) of Cu_3N decomposition to CuO as a function of NH_3 chemical yield (percent = 100x). The circled cross marker in red represents the NH_3 yield (x) observed in this study.

DOI: 10.1021/acs.inorgchem.5b00679
Inorg. Chem. 2015, 54, 6356−6362

and the amount of N_2 produced by this reaction (relative to NH_3). Unfortunately, we are presently unable to exactly calculate the free energies (ΔG_r) of reactions (7) and (8), because the free energy of formation (ΔG_f) of Cu_3N remains unknown.

In spite of the large enthalpic preference for exclusive N_2 production, this was not observed experimentally. On the basis of our observations that H_2O is required for Cu_3N decomposition to occur and that NH_3 is produced in 60% yield based on the initial amount of Cu_3N (x = 0.6, Table 2), we conclude that this reaction proceeds through a complex stoichiometry that involves the concomitant release of both N_2 and NH_3, according to eq 9. We are able to calculate the true thermodynamic cost of ammonia production by considering the difference in Gibb's free energies between reactions 9 and 7 ($\Delta\Delta G_{9-7}$), as follows:

$$\Delta\Delta G_{9-7} = \Delta G_9 - \Delta G_7 = x\Delta G^{f}_{NH_4^+(aq)} + x\Delta G^{f}_{HO^-(aq)} - \frac{5x}{2}\Delta G^{f}_{H_2O(l)} + \frac{x}{2}\Delta G^{f}_{N_2(g)} - \frac{3x}{4}\Delta G^{f}_{O_2(g)}$$

In this equation, $3\Delta G^{f}_{CuO(s)}$ and $\Delta G^{f}_{Cu_3N(s)}$ have been canceled out. In addition, by definition both $\Delta G^{f}_{N_2(g)}$ and $\Delta G^{f}_{O_2(g)}$ are zero under ideal or near-ideal conditions (25 °C, 1 atm). This yields

$$\Delta\Delta G_{9-7} = x\Delta G^{f}_{NH_4^+(aq)} + x\Delta G^{f}_{HO^-(aq)} - \frac{5x}{2}\Delta G^{f}_{H_2O(l)}$$
$$= -x(79\ \text{kJ/mol}) - x(157\ \text{kJ/mol}) + (5x/2)(237\ \text{kJ/mol})^{47} = x(358\ \text{kJ/mol})$$

Figure 7 shows a plot of $\Delta\Delta G_{9-7}$ as a function of chemical yield of NH_3 based on the initial amount of Cu_3N. The experimentally observed value of 60% is 72 kJ/mol less favorable by free energy compared to when (if) no ammonia is produced. This strongly indicates that the role of H_2O (and thus NH_3 production) is to facilitate the kinetics of the reaction by lowering the energy barrier for Cu_3N decomposition to CuO.

CONCLUSION

In summary, nanocrystalline Cu_3N was synthesized from nanocrystalline Cu_2O and one of two nitrogen sources, ammonia (NH_3) or urea (H_2NCONH_2). Using urea leads to slightly more phase-pure Cu_3N, as observed by XRD. In addition, the use of ammonia as the nitridation (ammonolysis) reagent requires a longer reaction time and higher temperature. TEM reveals that the cubic morphology of the initial Cu_2O nanocrystals is lost upon nitridation to Cu_3N. Nitridation with ammonia produces clusters of spherical particles whereas nitridation with urea produced a mixture of several different morphologies (rods, sheets, and aggregates). Electronic structure calculations of the DOS appear to underestimate, but agree with, the presence of a band gap of under 1 eV for both Cu_2O and Cu_3N phases.

Cu_3N nanocrystals spontaneously decompose to nanocrystalline CuO at room temperature. Control experiments show that both air (O_2, an oxidant) and moisture (H_2O, for hydrolysis to NH_3) are necessary for this transformation to take place. Cu_3N decomposition occurs within 15 days to produce substoichiometric amounts of ammonia. Specifically, ammonia was produced in 60% chemical yield during Cu_3N decomposition, as measured using the colorimetric indophenol method. Because Cu_3N decomposition requires H_2O and produces substoichiometric amounts of NH_3, we conclude that this reaction proceeds through a complex stoichiometry that involves the concomitant release of both N_2 and NH_3. This is a thermodynamically unfavorable outcome, strongly indicating that H_2O (and thus NH_3 production) facilitate the kinetics of the reaction by lowering the energy barrier for Cu_3N decomposition. Additional studies will be required to assess the potential reversibility and catalytic usefulness of this transformation.

ASSOCIATED CONTENT

Supporting Information

Additional XRD, selected area electron-diffraction (SAED) analyses, and solution-phase optical calibration data. The Supporting Information is available free of charge on the ACS Publications website at DOI: 10.1021/acs.inorgchem.5b00679.

AUTHOR INFORMATION

Corresponding Author

*E-mail: vela@iastate.edu.

Notes

The authors declare no competing financial interest.

ACKNOWLEDGMENTS

J.V. gratefully acknowledges the National Science Foundation for funding of this work through the Division of Materials Research, Solid State and Materials Chemistry program (NSF-DMR-1309510). M.A.W. thanks Yuemei Zhang for assistance with calculations.

REFERENCES

(1) Wang, D.; Li, Y. *Chem. Commun.* **2011**, *47*, 3604−3606.
(2) Xi, P.; Xu, Z.; Gao, D.; Chen, F.; Xue, D.; Tao, C.-L.; Chen, Z.-N. *RSC Adv.* **2014**, *4*, 14206−14209.
(3) Nakamura, T.; Hayashi, H.; Hanaoka, T.-A.; Ebina, T. *Inorg. Chem.* **2013**, *53*, 710−715.
(4) Wu, H.; Chen, W. *J. Am. Chem. Soc.* **2011**, *133*, 15236−15239.
(5) In, S.-I.; Vaughn, D. D., II; Schaak, R. E. *Angew. Chem., Int. Ed.* **2012**, *51*, 3915−3918.
(6) Lee, B. S.; Yi, M.; Chu, S. Y.; Lee, J. Y.; Kwon, H. R.; Lee, K. R.; Kang, D.; Kim, W. S.; Lim, H. B.; Lee, J.; Youn, H.-J.; Chi, D. Y.; Hur, N. H. *Chem. Commun.* **2010**, *46*, 3935−3937.
(7) Desmoulins-Krawiec, S.; Aymonier, C.; Loppinet-Serani, A.; Weill, F.; Gorsse, S.; Etourneau, J.; Cansell, F. *J. Mater. Chem.* **2004**, *14*, 228−232.
(8) Cansell, F.; Aymonier, C.; Loppinet-Serani, A. *Curr. Opin. Solid State Mater. Sci.* **2003**, *7*, 331−340.
(9) Cansell, F.; Chevalier, B.; Demourgeues, A.; Etourneau, J.; Even, C.; Garrabos, Y.; Pessey, V.; Petit, S.; Tressaud, A.; Weill, F. *J. Mater. Chem.* **1999**, *9*, 67−75.
(10) Choi, J.; Gillan, E. G. *Inorg. Chem.* **2005**, *44*, 7385−7393.
(11) Trivedi, M.; Singh, G.; Kumar, A.; Rath, N. P. *RSC Adv.* **2014**, *4*, 34110−34116.
(12) Paniconi, G.; Stoeva, Z.; Doberstein, H.; Smith, R. I.; Gallagher, B. L.; Gregory, D. H. *Solid State Sci.* **2007**, *9*, 907−913.
(13) Gordillo, N.; Gonzalez-Arrabal, R.; Martin-Gonzalez, M. S.; Olivares, J.; Rivera, A.; Briones, F.; Agulló-López, F.; Boerma, D. O. *J. Cryst. Growth* **2008**, *310*, 4362−4367.
(14) Hadian, F.; Rahmati, A.; Movla, H.; Khaksar, M. *Vacuum* **2012**, *86*, 1067−1072.

DOI: 10.1021/acs.inorgchem.5b00679
Inorg. Chem. 2015, 54, 6356−6362

(15) Gordillo, N.; Rivera, A.; Grötzschel, R.; Munnik, F.; Güttler, D.; Crespillo, M. L.; Agulló-López, F.; Gonzalez-Arrabal, R. *J. Phys. D: Appl. Phys.* **2010**, *43*, 345301−1−9.
(16) Gonzalez-Arrabal, R.; Gordillo, N.; Martin-Gonzalez, M. S.; Ruiz-Bustos, R.; Agulló-López, F. *J. Appl. Phys.* **2010**, *107*, 103513−1−7.
(17) Deshmukh, R.; Schubert, U. *Eur. J. Inorg. Chem.* **2013**, *14*, 2498−2504.
(18) Deshmukh, R.; Schubert, U. *J. Mater. Chem.* **2011**, *21*, 18534−18536.
(19) Baiker, A.; Maciejewski, M. *J. Chem. Soc., Faraday Trans. 1* **1984**, *80*, 2331−2341.
(20) Filipič, G.; Cvelbar, U. *Nanotechnology* **2012**, *23*, 194001−1−16.
(21) Zhang, Q.; Zhang, K.; Xu, D.; Yang, G.; Huang, H.; Nie, F.; Liu, C.; Yang, S. *Prog. Mater. Sci.* **2014**, *60*, 208−337.
(22) Kuo, C.-H.; Huang, M. H. *Nano Today* **2010**, *5*, 106−116.
(23) Lignier, P.; Bellabarba, R.; Tooze, R. P. *Chem. Soc. Rev.* **2012**, *41*, 1708−1720.
(24) Fan, X. Y.; Wu, Z. G.; Yan, P. X.; Geng, B. S.; Li, H. J.; Li, C.; Zhang, P. J. *Mater. Lett.* **2008**, *62*, 1805−1808.
(25) Lesch, N.; Karduck, P.; Cremer, R.; Richthofen, A. V. *Fresenius J. Anal. Chem.* **1998**, *361*, 604−607.
(26) Yue, G. H.; Yan, P. X.; Wang, J. *J. Cryst. Growth* **2005**, *274*, 464−468.
(27) Asano, M.; Umeda, K.; Tasaki, A. *Jpn. J. Appl. Phys.* **1990**, *29*, 1985−1986.
(28) Wang, Z.; Wang, H.; Wang, L.; Pan, L. *Cryst. Res. Technol.* **2009**, *44*, 624−628.
(29) Weatherburn, M. W. *Anal. Chem.* **1967**, *39*, 971−974.
(30) Searle, P. L. *Analyst* **1984**, *109*, 549−568.
(31) Kresse, G.; Furthmüller, J. *Comput. Mater. Sci.* **1996**, *6*, 15−50.
(32) Kresse, G. *Phys. Rev. B* **1996**, *54*, 11169−11186.
(33) Kresse, G.; Joubert, D. *Phys. Rev. B* **1999**, *59*, 1758−1775.
(34) Monkhorst, H. J.; Pack, J. D. *Phys. Rev. B* **1976**, *13*, 5188−5192.
(35) Blöchl, P. E. *Phys. Rev. B* **1994**, *50*, 17953−17979.
(36) Perdew, J. P.; Burke, K.; Ernzerhof, M. *Phys. Rev. Lett.* **1996**, *77*, 3865−3868.
(37) Scanlon, D.; Walsh, A.; Morgan, B.; Watson, G.; Payne, D.; Egdell, R. *Phys. Rev. B* **2009**, *79*, 035101−1−7.
(38) Raebiger, H.; Lany, S.; Zunger, A. *Phys. Rev. B* **2007**, *76*, 045209−1−5.
(39) Xiao, J.; Li, Y.; Jiang, A. *J. Mater. Sci. Technol.* **2011**, *27*, 403−407.
(40) Ching, W.; Xu, Y.-N.; Wong, K. *Phys. Rev. B* **1989**, *40*, 7684−7695.
(41) Hahn, U.; Weber, W. *Phys. Rev. B* **1996**, *53*, 12684−12693.
(42) Elliott, R. *Phys. Rev.* **1957**, *108*, 1384−1389.
(43) Marabelli, F.; Parravicini, G. B.; Salghetti-Drioli, F. *Phys. Rev. B* **1995**, *52*, 1433−1436.
(44) Serin, N.; Serin, T.; Horzum, Ş.; Çelik, Y. *Semicond. Sci. Technol.* **2005**, *20*, 398−401.
(45) Ekuma, C. E.; Anisimov, V. I.; Moreno, J.; Jarrell, M. *Eur. Phys. J. B* **2014**, *87*, 23−1−6.
(46) Vela, J.; Stoian, S.; Flaschenriem, C. J.; Münck, E.; Holland, P. L. *J. Am. Chem. Soc.* **2004**, *126*, 4522−4523.
(47) Yandulov, D. V.; Schrock, R. R. *Science* **2003**, *301*, 76−78.
(48) Elder, S. H.; DiSalvo, F. J.; Topor, L.; Navrotsky, A. *Chem. Mater.* **1993**, *5*, 1545−1553.
(49) Caskey, C. M.; Richards, R. M.; Ginleya, D. S.; Zakutayeva, A. *Mater. Horiz.* **2014**, *1*, 424−430.
(50) *CRC Handbook of Chemistry and Physics*, 95th ed.; CRC: Boca Raton, FL, 2013.

DOI: 10.1021/acs.inorgchem.5b00679
Inorg. Chem. 2015, 54, 6356−6362